

Advances in LS-DYNA[®] Metal Forming (II)

Xinhai Zhu, Li Zhang & Yuzhong Xiao

Livermore Software Technology Corporation

Abstract

Some of the new features developed since the last conference will be discussed.

- 1) *Implementation of Stoughton's Non-Associate Flow Model (*MAT_260A)
Strain rate sensitive, non-associated flow material model suitable for metal forming simulation.*
- 2) *Implementation of Mohr's Non-Associate Flow Model (*MAT_260B)
Strain rate sensitive and temperature softening effect coupled with a non-associated flow rule, combined with a ductile fracture model based on Hosford-Coulomb fracture initiation model, suitable for metal forming and crash simulation.*
- 3) *Best fitting of meshed (including STL) parts with *CONTROL_FORMING_BESTFIT
Correlation study of simulated springback with scanned STL file made easy.*
- 4) *Tool mesh checking/fixing and physical offset of tools (*CONTROL_FORMING_AUTOCHECK)
This feature fixes tooling meshes arising from bad tool CAD surfaces, automatically make tool normal consistent and in required orientation, and offsets the tool mesh to create an opposite side of the tool.*
- 5) *Formability Index (F.I.) extension to *MAT_036, *MAT_125 and *MAT_226.
Predictions of sheet metal failure under non-linear strain paths are extended to aforementioned material models.*
- 6) *Implementation of a Cyclic Fatigue Modeling (*MAT_165B)
A mixed isotropic and kinematic hardening model suitable for small strain cyclic fatigue modeling.*

*MAT_260A

This material model is implemented based on non-associated flow rule models (Stoughton 2002 and 2004) and is applicable to both shell and solid elements. Strain rate sensitivity can be included using a load curve.

In non-associated flow rule, material yield function does not equal to the plastic flow potential. According to Thomas B. Stoughton's paper titled "A non-associated flow rule for sheet metal forming" in 2002 International Journal of Plasticity 18, 687-714, and "A pressuresensitive yield criterion under a non-associated flow rule for sheet metal forming" in 2004 International Journal of Plasticity 20, 705-731, plastic potential is defined by:

$$\bar{\sigma}_p = \sqrt[3]{\sigma_{11}^2 + \lambda_p \sigma_{22}^2 - 2\nu_p \sigma_{11} \sigma_{22} + 2\rho_p \sigma_{12}^2}$$

where σ_{ij} is the stress tensor component; where,

$$\lambda_p = \frac{1 + \frac{1}{r_{90}}}{1 + \frac{1}{r_0}},$$

$$v_p = \frac{r_0}{1 + r_0},$$

$$\rho_p = \frac{\frac{1}{r_0} + \frac{1}{r_{90}}}{1 + \frac{1}{r_0}} \left(\frac{1}{2} + r_{45} \right).$$

where, r_0 , r_{45} , r_{90} are Lankford parameters in the rolling (0), the diagonal (45) and the transverse (90) directions, respectively.

Yield function is defined by:

$$\bar{\sigma}_y = \sqrt[3]{\sigma_{11}^2 + \lambda_y \sigma_{22}^2 - 2v_y \sigma_{11} \sigma_{22} + 2\rho_y \sigma_{12}^2}$$

where,

$$\lambda_y = \left(\frac{\sigma_0}{\sigma_{90}} \right)^2,$$

$$v_y = \frac{1}{2} \left[1 + \lambda_y - \left(\frac{\sigma_0}{\sigma_b} \right)^2 \right],$$

$$\rho_y = \frac{1}{2} \left[\left(\frac{2\sigma_0}{\sigma_{45}} \right)^2 - \left(\frac{\sigma_0}{\sigma_b} \right)^2 \right].$$

where, σ_0 , σ_{45} , σ_{90} are the initial yield stresses from uniaxial tension tests in the rolling (0), the diagonal (45), and the transverse (90) directions, respectively. σ_b is the initial yield stress from an equi-biaxial stretching test.

The required stress-strain hardening curve (LCIDS) is from uniaxial tension test along the rolling direction. Strain rate sensitivity is implemented as an option, by defining a curve (LCIDV) of strain rates vs. stress scale factors, see Figure 2.

The variable SCALE can be used in speeding up the simulation while equalizing the strain rate effect. For example, if the real, physical pulling speed is at 15 mm/s but running at this speed will take a long time, one could increase the pulling speed to 500 mm/s while setting the SCALE to 0.03, resulting in the same results as those from 15 mm/s with the benefit of greatly reduced computational time.

In Figure 1, uniaxial tension tests were done on a single shell element. Strain rate effect LCIDV is input as shown in Figure 2. In Figure 3, pulling stress vs. strain from various test conditions are compared with input stress-strain curve A. In summary, using the parameter SCALE, the element can be pulled much faster (500 mm/s vs. 15 mm/s) but achieve the same stress vs. strain results, the same strain rates (history variable #5), and the same strain rate scale factor (history variable #6 in Figure 4). Simulation speed can be improved further with increased mass scaling (-1.0*dt2ms) without affecting the results, see Figure 5.

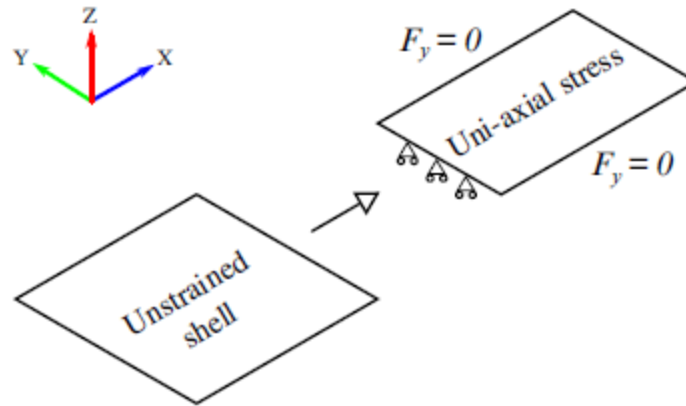


Figure 1. Uniaxial tension tests on a single shell element.

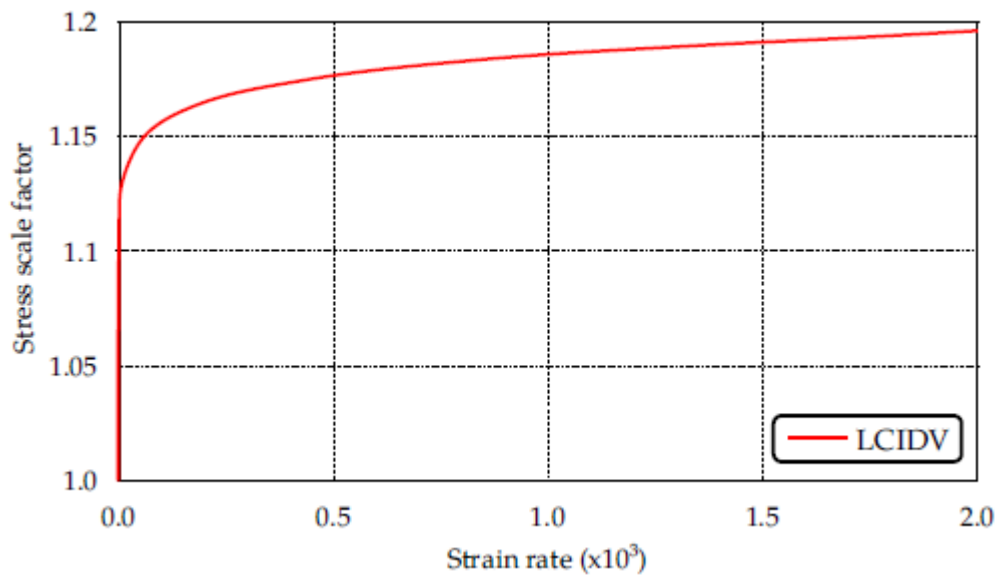


Figure 2. Input LCIDV.

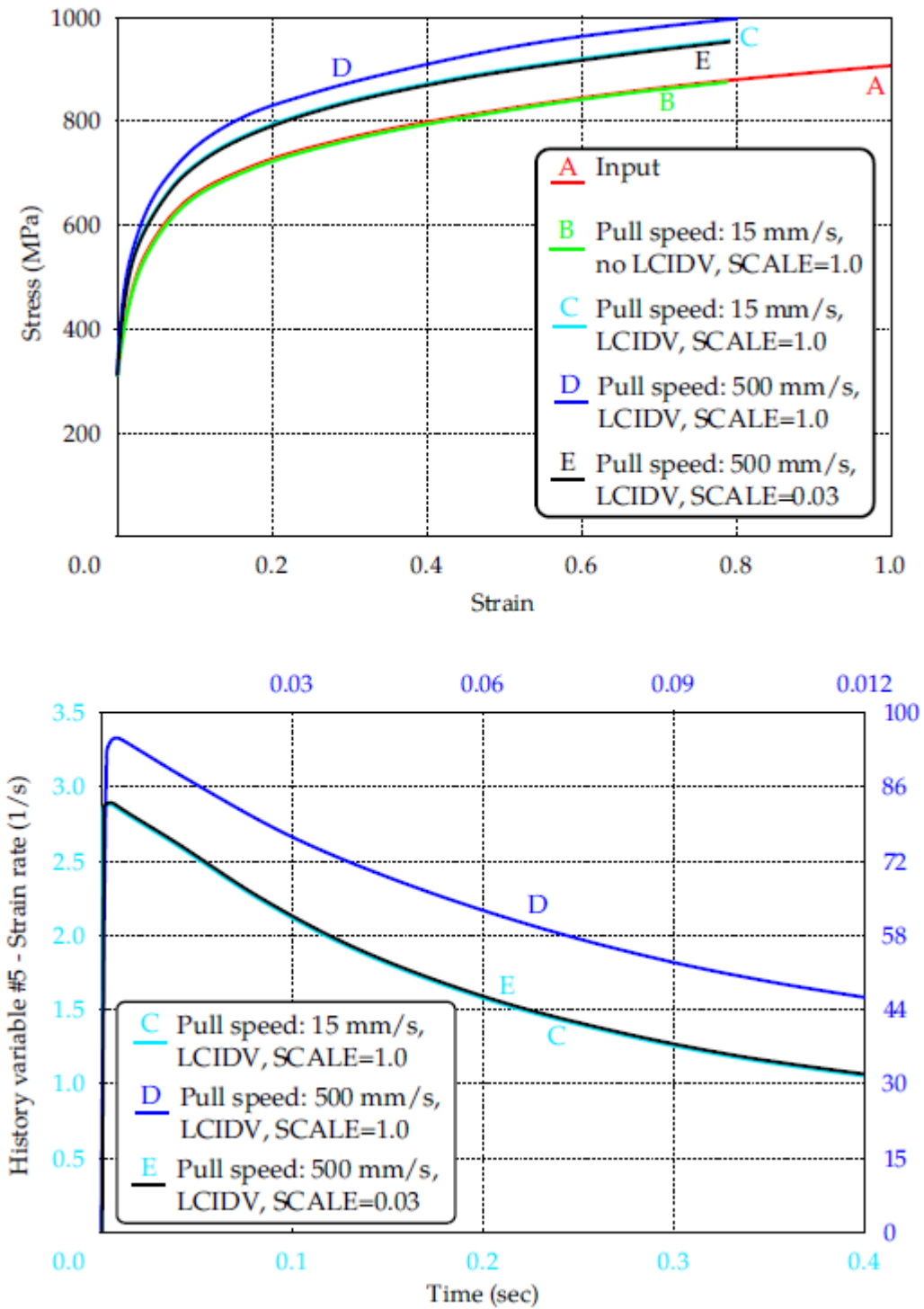


Figure 3. Recovered stress-strain curve (top) and strain rates (bottom) under various conditions shown.

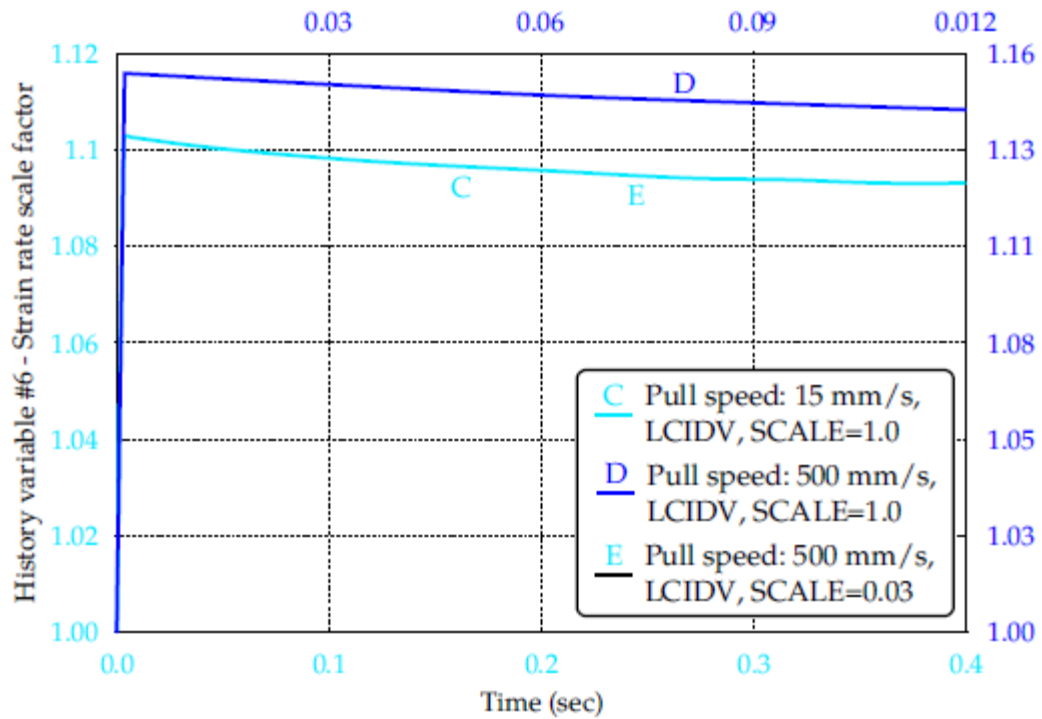


Figure 4. Recovered strain rate scale factors under various conditions shown.

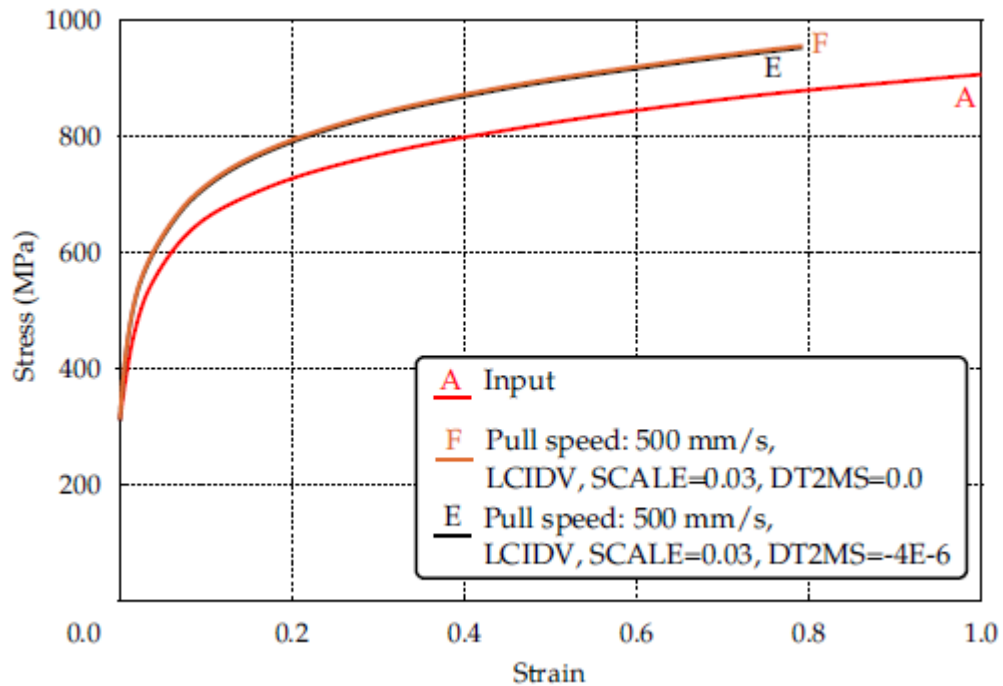


Figure 5. Effect of mass scaling (-1.0*dt2ms).

***MAT_260B**

This material model is implemented based on the papers by Mohr, D., et al.(2010) and Roth, C.C., Mohr, D. (2014). The Johnson-Cook plasticity model of strain hardening, strain rate hardening, and temperature soften effect is modified with a mixed Swift-Voce strain hardening function, coupled with a non-associated flow rule which accounts for the difference between directional dependency of the r -values (planar anisotropic), and planar isotropic material response of certain Advanced High Strength Steels (AHSS). A ductile fracture model is included based on Hosford-Coulomb fracture initiation model. This model applies to both shell and solid elements.

To make this material model more general and flexible, three load curves are used to define the three components of the deformation resistance. A load curve (LCIDS) is used to describe the strain hardening:

$$\text{LCIDS: } \left(\alpha(A(\bar{\epsilon}_{pl} + \epsilon_0)^n) + (1 - \alpha) \left(k_0 + Q(1 - e^{-\beta\bar{\epsilon}_{pl}}) \right) \right)$$

Strain rate is described by a load curve LCIDV (stress scale factor vs. strain rates, Figure 6 middle), which scales the stresses based on the strain rates during a simulation:

$$\text{LCIDV: } \left(1 + C \ln \left(\frac{\dot{\bar{\epsilon}}_{pl}}{\dot{\epsilon}_0} \right) \right)$$

The temperature softening effect is defined by another load curve LCIDT (stress scale factor vs. temperature, Figure M260B-1 bottom), which scales the stresses based on the temperatures during the simulation:

$$\text{LCIDT: } \left(1 - \left(\frac{T - T_r}{T_m - T_r} \right)^m \right)$$

The temperature effect is a self-contained model, in other words, it does not require thermal exchange with the environment, and it calculates temperatures based on plastic strain and strain rate.

The temperature evolution is determined with:

$$dT = \omega \left[\frac{\dot{\bar{\epsilon}}_{pl}}{\dot{\epsilon}_0} \right] \frac{\eta k}{\rho C_p} \bar{\sigma} d\bar{\epsilon}_{pl}$$

Where ηk (ETA) is Taylor-Quinney coefficient, ρ (R0) is the mass density and C_p (CP) is the heat capacity; also where,

$$\omega[\dot{\bar{\epsilon}}_{pl}] = \begin{cases} 0 & \text{for } \dot{\bar{\epsilon}}_{pl} < \dot{\epsilon}_{it} \\ \frac{(\dot{\bar{\epsilon}}_{pl} - \dot{\epsilon}_{it})^2 (3\dot{\epsilon}_a - 2\dot{\bar{\epsilon}}_{pl} - \dot{\epsilon}_{it})}{(\dot{\epsilon}_a - \dot{\epsilon}_{it})^3} & \text{for } \dot{\epsilon}_{it} \leq \dot{\bar{\epsilon}}_{pl} \leq \dot{\epsilon}_a \\ 1 & \text{for } \dot{\epsilon}_a < \dot{\bar{\epsilon}}_{pl} \end{cases}$$

where $\dot{\epsilon}_{it} > 0$ and $\dot{\epsilon}_a > \dot{\epsilon}_{it}$ define the limits of the respective domains of isothermal and adiabatic conditions ($\dot{\epsilon}_a = \text{DEPSAD}$). For simplification, $\dot{\epsilon}_{it} = \dot{\epsilon}_0(\text{DEPS0})$.

As shown in a single shell element uniaxial stretching (Figure 6), the general effect of the LCIDV is to elevate the strain hardening behavior as the strain rate increases (curve “D” in Figure 7 top), while the effect of the LCIDT is strain softening as temperature rises (curve “C” in Figure 7 top). A combined effect of both LCIDV and LCIDT may result in strain hardening initially before temperature rise enough to cause the strain softening in the model (curve “E” in Figure 7 top). The temperature and strain rates calculated for each element can be viewed with history variables #4 and #5 (curves “C” and “D” in Figure 7 bottom), respectively, while the strain rate scale factors and temperature scale factors can be viewed with history variable #6 and #7, respectively.

An extension of the Hosford-Coulomb fracture initiation model is used to account for the effect of strain rate on ductile fracture. The damage accumulation is calculated through history variable #3, and fracture occurs at an equivalent plastic strain $\epsilon_f^{\bar{}}$ when the variable reaches 1.0:

$$\int_0^{\epsilon_f^{\bar{}}} \frac{d\bar{\epsilon}_{pl}}{\bar{\epsilon}_f^{pr}[\eta, \bar{\theta}]} = 1$$

Where $\bar{\epsilon}_f^{pr}$, η , $\bar{\theta}$ are strain to fracture, stress triaxiality and the Lode parameter, respectively.

The fracture parameters A, B0, GAMMA, C, N (a, b_0, γ, c, n) are indicated in the following equations. Strain to fracture for proportional load:

$$\bar{\epsilon}_f^{pr}[\eta, \bar{\theta}] = b(1 + c)^{\frac{1}{n}} \left(\left\{ \frac{1}{2} ((f_1 - f_2)^a + (f_2 - f_3)^a + (f_1 - f_3)^a) \right\}^{\frac{1}{a}} + c(2\eta + f_1 + f_3) \right)^{\frac{1}{n}}$$

where a is the Hosford exponent, c is the friction coefficient controlling the effect of triaxiality, n is the stress state sensitivity.

The Lode angle parameter dependent trigonometric functions:

$$f_1[\bar{\theta}] = \frac{2}{3} \cos\left[\frac{\pi}{6}(1 - \bar{\theta})\right], \quad f_2[\bar{\theta}] = \frac{2}{3} \cos\left[\frac{\pi}{6}(3 + \bar{\theta})\right], \quad f_3[\bar{\theta}] = -\frac{2}{3} \cos\left[\frac{\pi}{6}(1 + \bar{\theta})\right]$$

and coefficient b (strain to fracture for uniaxial or equi-biaxial stretching):

$$b = \begin{cases} b_0 & \text{for } \dot{\epsilon}_p < \dot{\epsilon}_0 \\ b_0 \left(1 + \gamma \ln \left[\frac{\dot{\epsilon}_p}{\dot{\epsilon}_0} \right] \right) & \text{for } \dot{\epsilon}_p > \dot{\epsilon}_0 \end{cases}$$

where γ is the strain rate sensitivity. Damage accumulation is stored in history variable #3, and failure occurs when this variable reaches the value of 1.0.

Bestfitting of Meshes to Measurement (STL)

This keyword is created to transform one mesh to another so they maximally coincide. It applies to shell elements only.

In springback prediction and compensation process simulation, there is always a need to assess the accuracy of the springback prediction using physical white-light scanned parts. Scanned parts are typically given in the STL format, which can be imported into LS-PrePost[®] and written back out as a keyword mesh file for use in this keyword.

The converted scanned keyword file can be used as a target mesh. The predicted springback mesh (with *NODE, *ELEMENT_SHELL, *CONSTRAIN_ADAPTIVITY cards only) can be included in the input file using *INCLUDE. The best-fit program uses an iterative least-squares method to minimize the separation distances between the two parts, eventually transforming the springback mesh (source) into the position of the target mesh (scan). The normal distances between the two parts are calculated after the best-fitting, and stored as thickness values in a file bestfit.out, which is essentially a dynain file.

It is suggested that NSETS and NSETT be used to initially align the source mesh to the target mesh before a best-fit simulation is performed (Figure8).

Both positive and negative distances are calculated and stored as the Thickness (Figure 9). For areas where no corresponding meshes can be found between the two parts, the distances are set to nearly zero. The fitting accuracy is within 0.02mm. In addition, the coarser mesh should be selected as the target mesh for optimal computational speed.

The fitted mesh and target mesh parts can both be imported into LS-PrePost. Using the SPLANE feature in LS-PrePost, multiple sections can be cut on both parts to assess springback deviations on a cut-section basis.

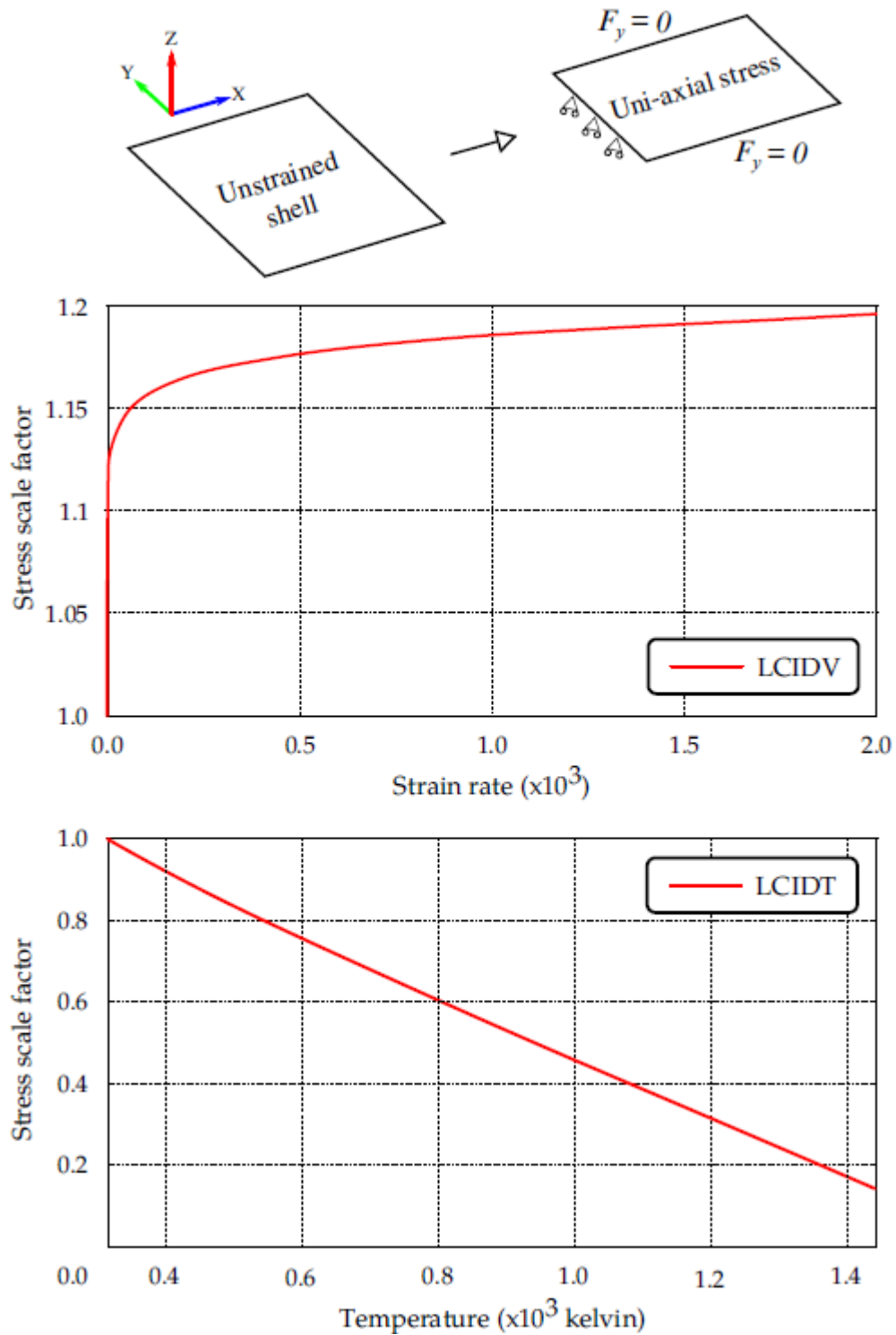


Figure 6. Uniaxial stretching on a single shell element; Input curves LCIDV and LCIDT.

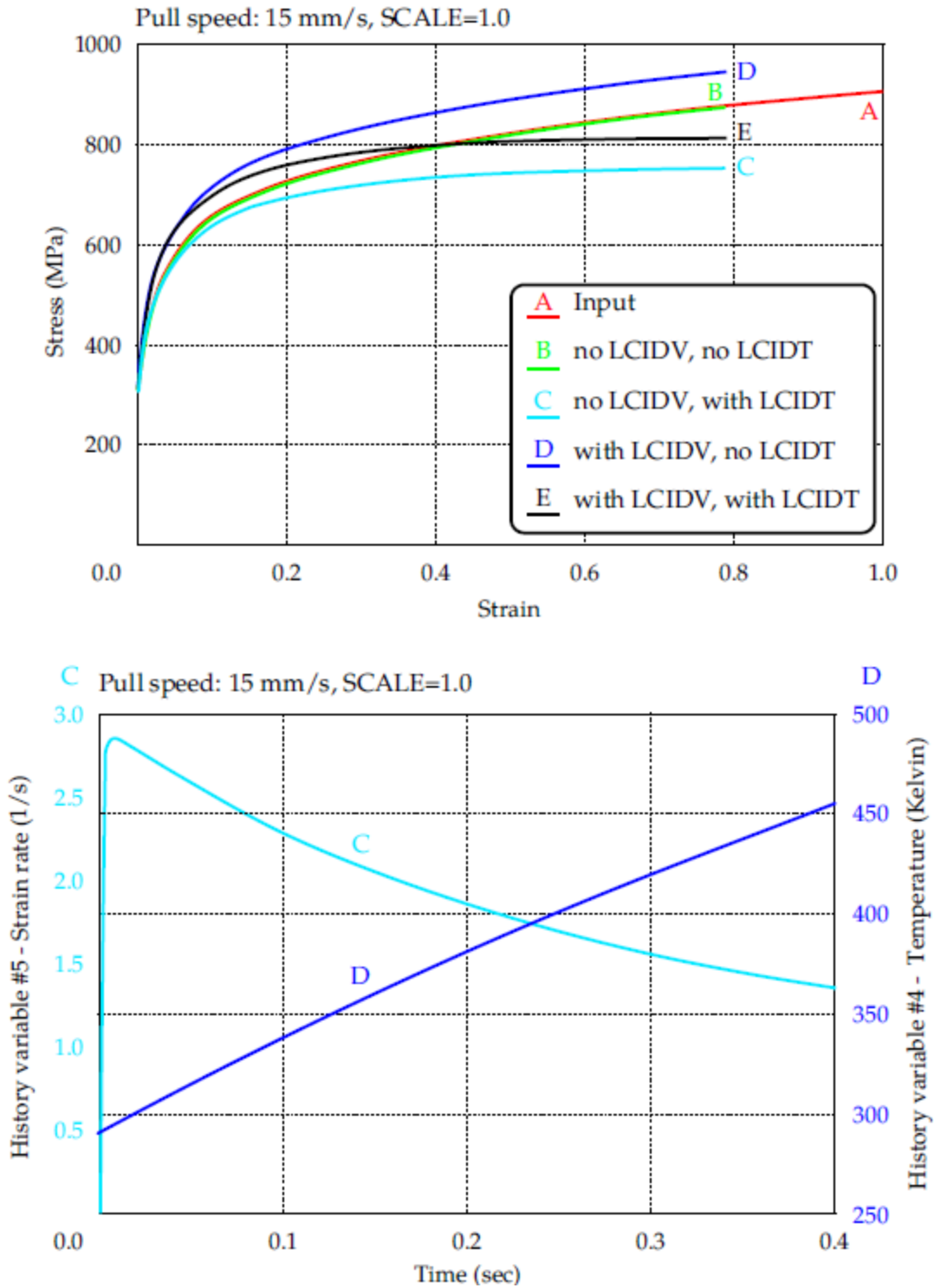


Figure 7. Results of a single element uniaxial stretching - stress-strain curves (top), strain rates and temperature history under various conditions.

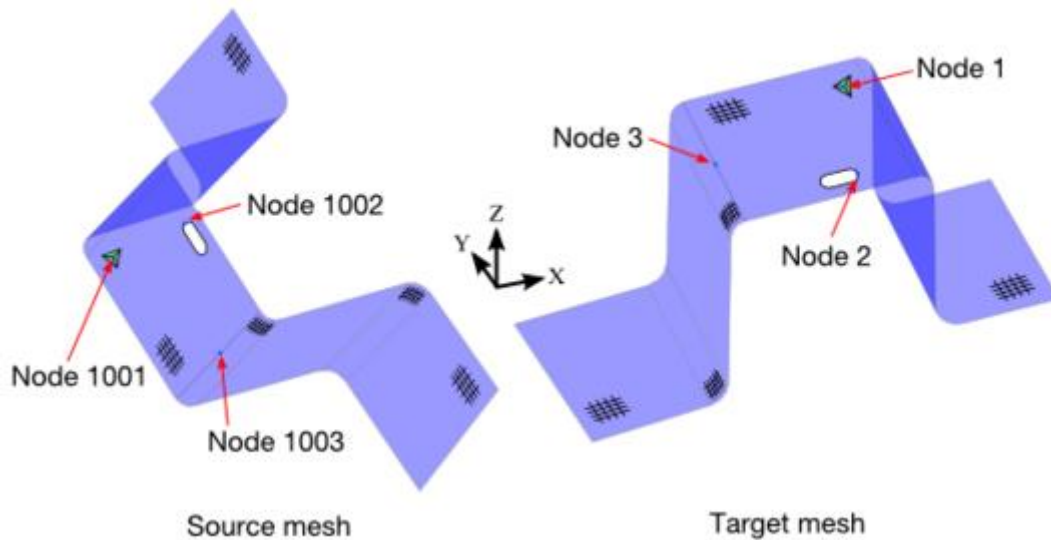


Figure 8. Bestfitting of two parts using NODE1, NODE2 and NODE3.

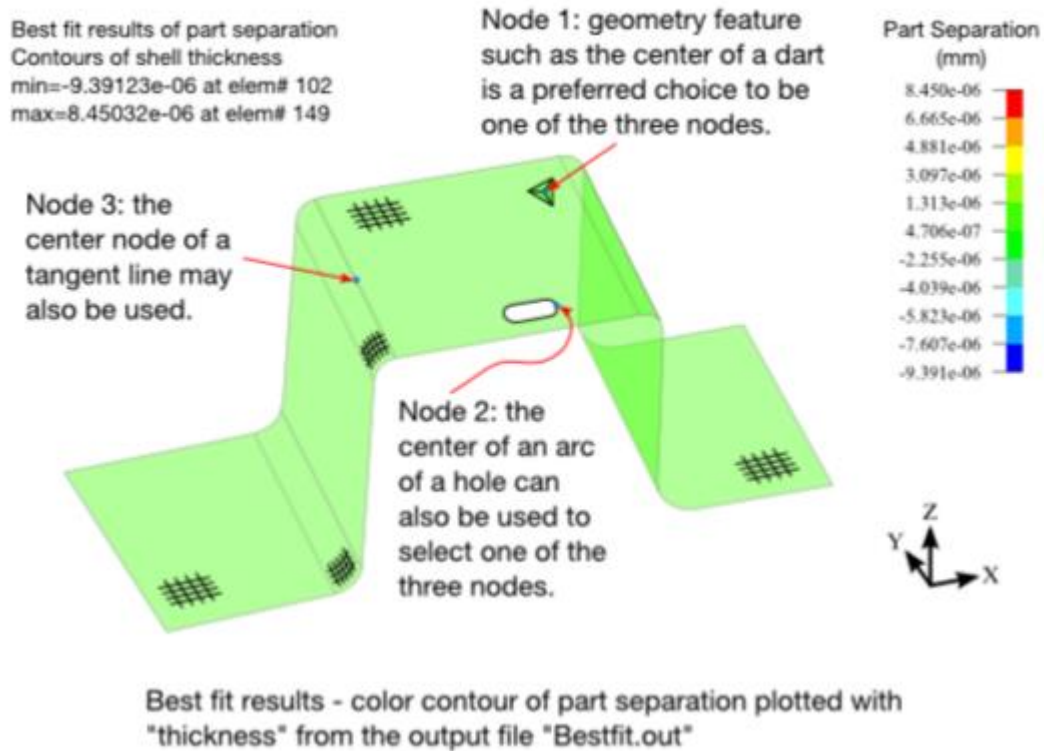


Figure 9. Bestfitted results of two parts using NODE1, NODE2 and NODE3.

Tool Mesh Fixing and Physical Offset of Stamping Tools

A newly created keyword (*CONTROL_FORMING_AUTOCHECK) checks the tooling mesh (rigid bodies, shells only) for duplicated elements, overlapping elements, skinny/long elements, degenerated elements, disconnected elements, and inconsistent element normal vectors. This feature also automatically orients each tool's element normal vectors so that they face the blank. Additionally an offset can be specified to create another tool (tool physical offset) based on the corrected tool meshes.

Some cases of incoming bad tooling meshes which can be corrected by this keyword are shown in Figure 10. This keyword can be inserted anywhere in the input deck. To include the corrected tooling mesh into the d3plot the ICHECK field (refer to the User's Manual I) must be defined. The corrected mesh is written to a file "rigid_offset_before.inc" if IOFFSET and IOUTPUT are defined.

When IOFFSET = 1 and IOUTPUT is defined, the tool meshes will first be checked, corrected, and reoriented correctly towards the blank. Then the tool is offset by an amount of $0.5|MST|$ either on the same or opposite side of the blank, depending on the signs of the MST field on the *CONTACT_FORMING_... card (Figure 11). A new keyword file, "rigid_offset.inc" file, will be output as containing the corrected, reoriented, and offset tooling mesh.

The tool offset feature is now available in LS-PrePost 4.2 under Application → MetalForming → Easy Setup, where the *offset from Die* button under *Binder* can be used to create offset tools.

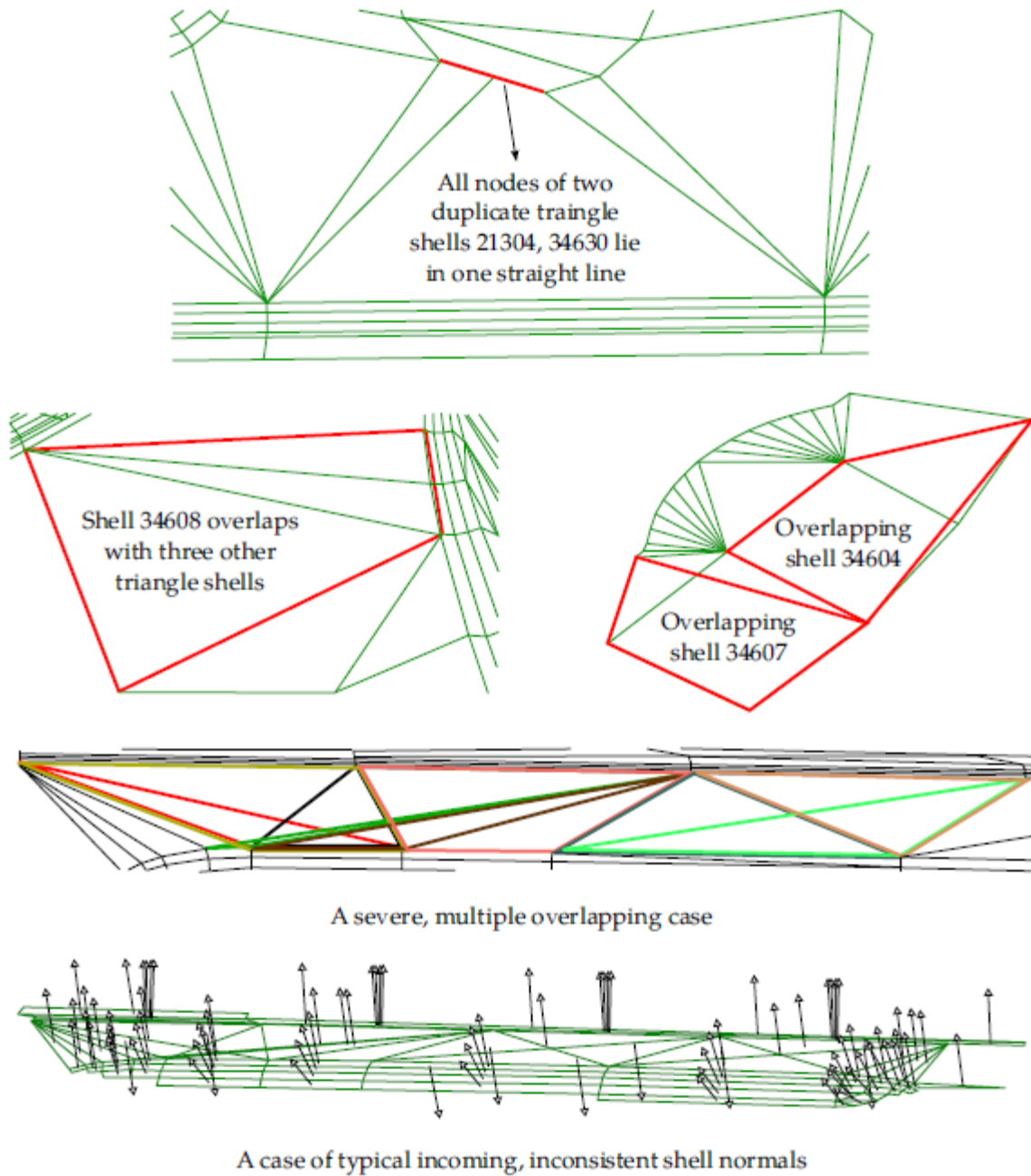


Figure 10. Some examples of the tooling mesh problems fixed by this keyword.

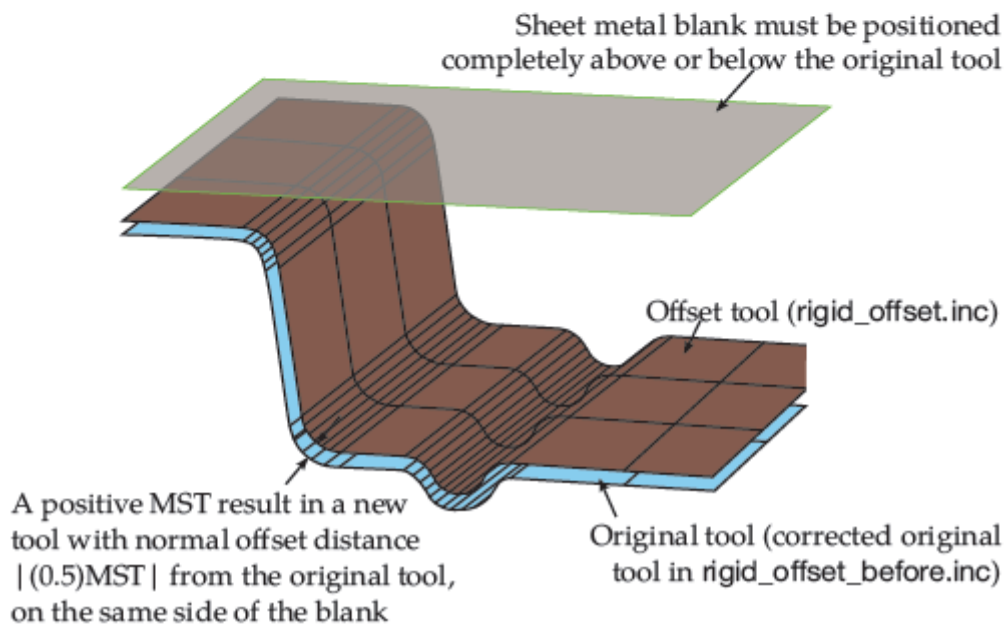
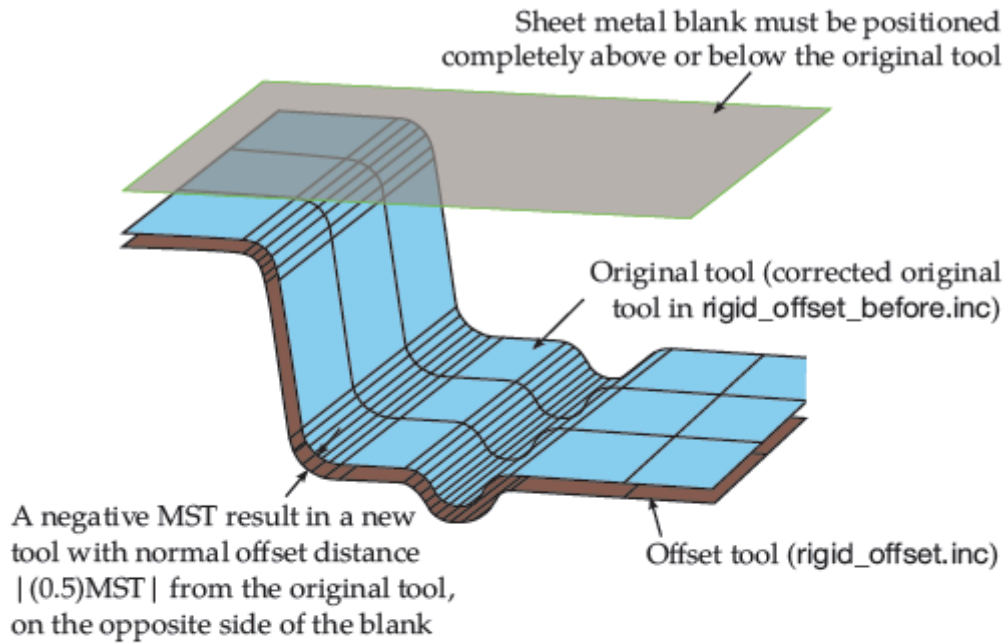


Figure 11. Tooling offset using the MST value defined in *CONTACT_FORMING_...

Failure Criterion in *MAT_036, *MAT_125 and *MAT_226

The NLP option estimates failure using the Formability Index (F.I.), which accounts for the non-linear strain paths seen in metal forming applications. A load curve which describes the traditional FLD should be input in the appropriate field (for example, the variable NLP in card 3 for *MAT_036) when using this option. The NLP option is implemented in *MAT_036, *MAT_125 and *MAT_226, in addition to *MAT_037. In this paper, we will briefly summarize the NLP option for *MAT_036, and users are referred to the User's Manual II for the rest of the material models aforementioned.

Based on the traditional Forming Limit Diagram (FLD) for the linear strain path, the Formability Index (F.I.) is calculated for every element in the model throughout the simulation duration. The entire F.I. time history for every element is stored in history variable #1 in d3plot files, accessible from Post/History menu in LS-PrePost v4.0. In addition to the F.I. output, other useful information stored in other history variables can be found as follows,

1. Formability Index: #1
2. Strain ratio (in-plane minor strain/major strain): #2
3. Effective strain from the planar isotropic assumption: #3

Shown in Figures 12, 13 and 14, predictions and validations of forming limit curves (FLC) of various nonlinear strain paths on a single shell element was done using this new option, for an Aluminum alloy with $r_{00} = 0.8$, $r_{45} = 0.6$, $r_{90} = 0.55$, and yield at 130.0 MPa. In each case, the element is further strained in three different paths (uniaxial stress – U.A., plane strain – P.S., and equi-biaxial strain – E.B.) separately, following a pre-straining in uniaxial, plane strain and equi-biaxial strain state, respectively. The forming limits are determined at the end of the secondary straining for each path, when the F.I. has reached the value of 1.0. It is seen that the predicted FLCs (dashed curves) in case of the nonlinear strain paths are totally different from the FLCs under the linear strain paths. It is noted that the current predicted FLCs under nonlinear strain path are obtained by connecting the ends of the three distinctive strain paths. More detailed FLCs can be obtained by straining the elements in more paths between U.A. and P.S. and between P.S. and E.B.

Typically, to assess sheet formability, F.I. contour of the entire part should be plotted. Based on the contour plot, non-linear strain path and the F.I. time history of a few elements in the area of concern can be plotted for further study. These plots are shown in Figures 15 and 16.

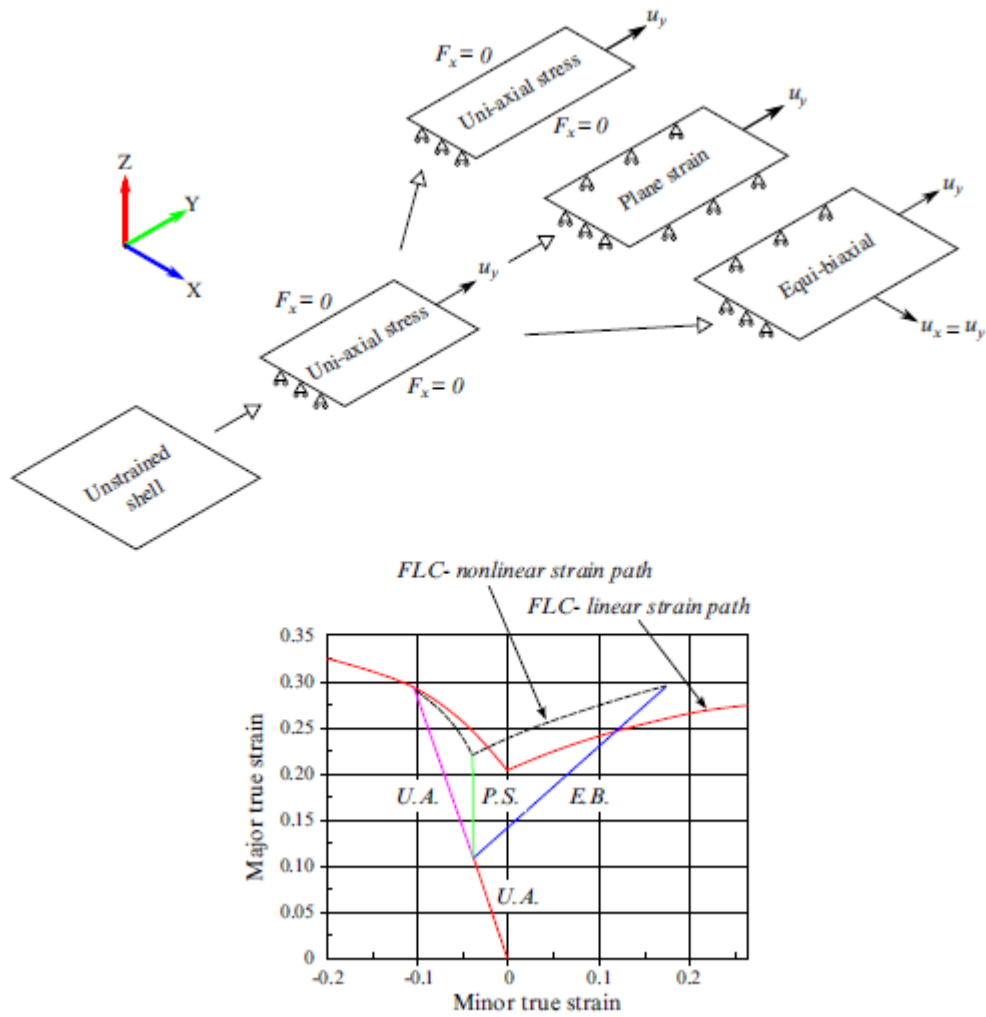


Figure 12. Nonlinear FLD prediction with uniaxial pre-straining.

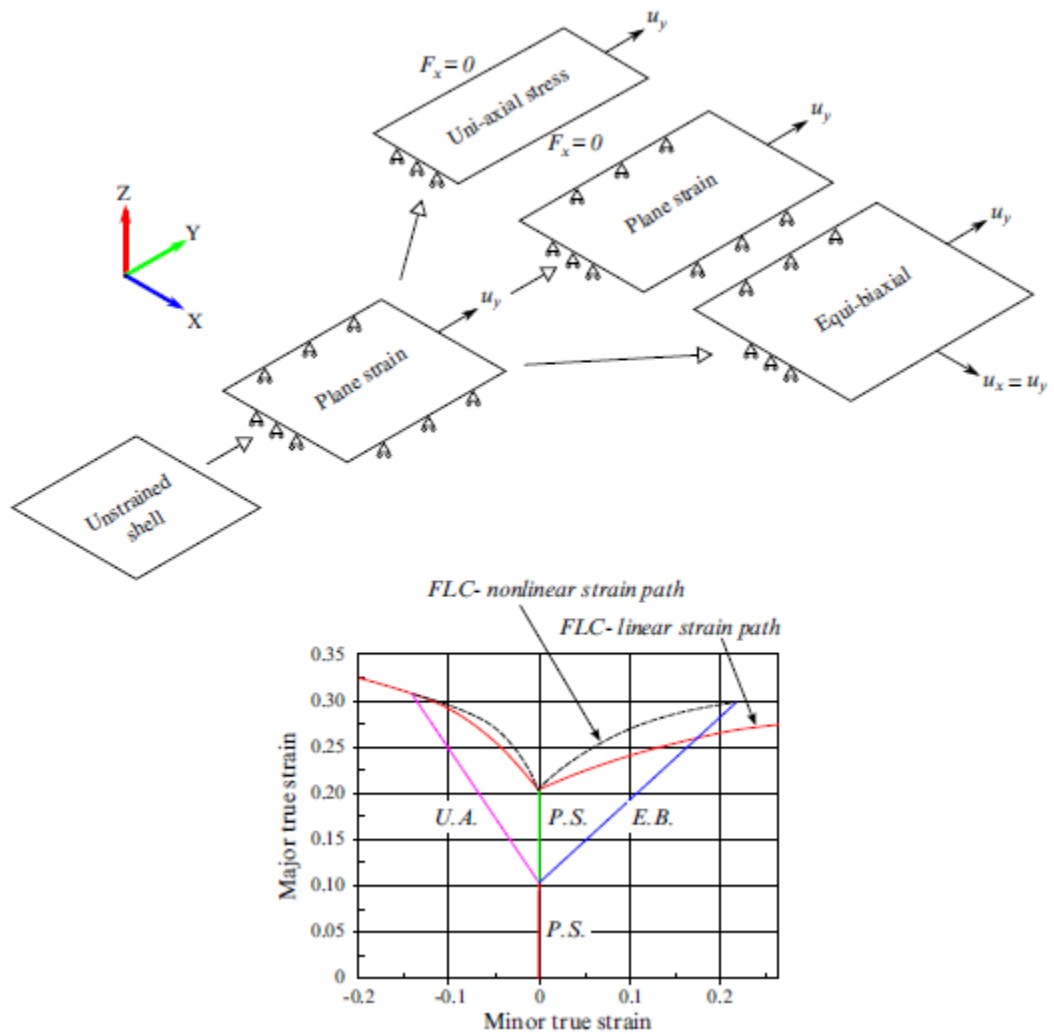


Figure 13. Nonlinear FLD prediction with plane strain pre-straining.

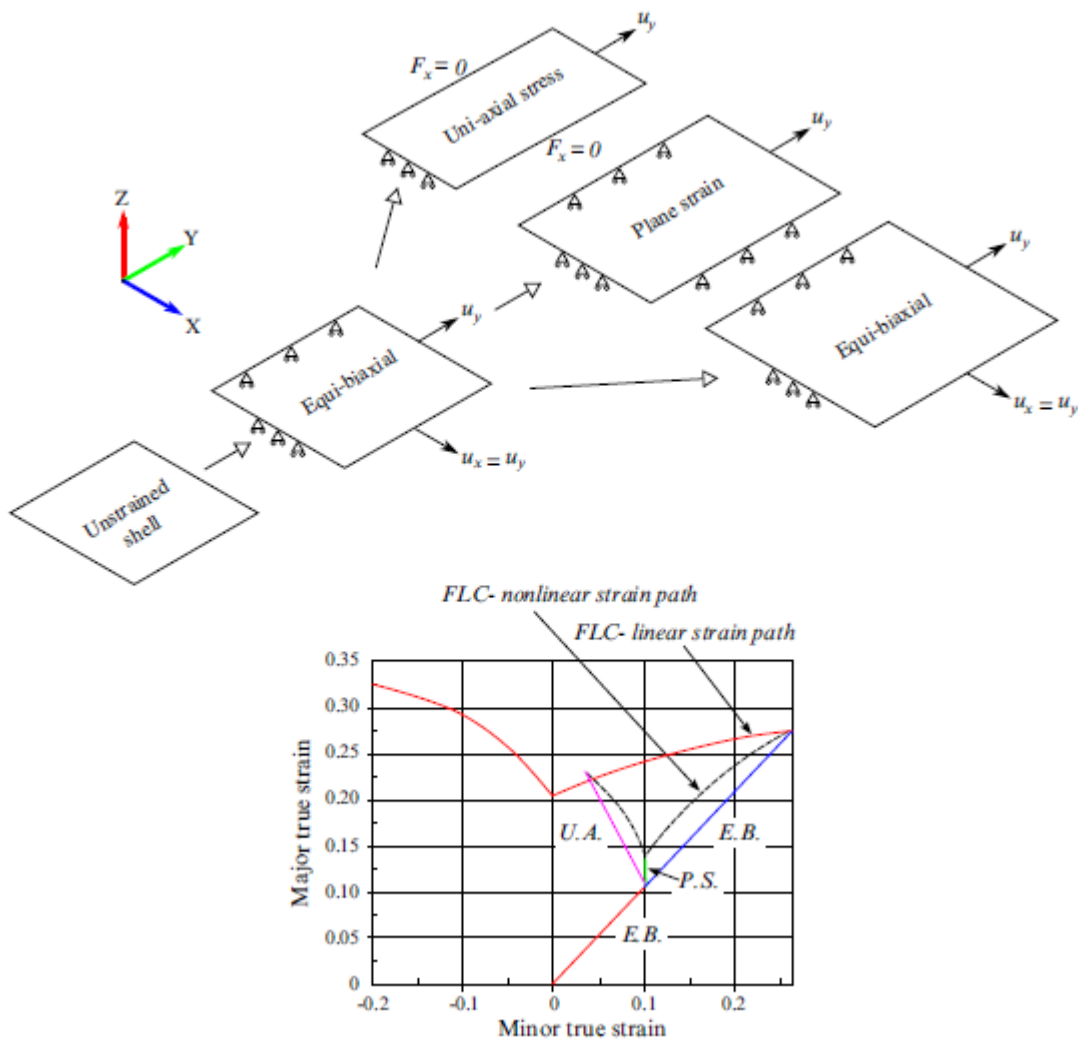


Figure 14. Nonlinear FLD prediction with equi-biaxial pre-straining.

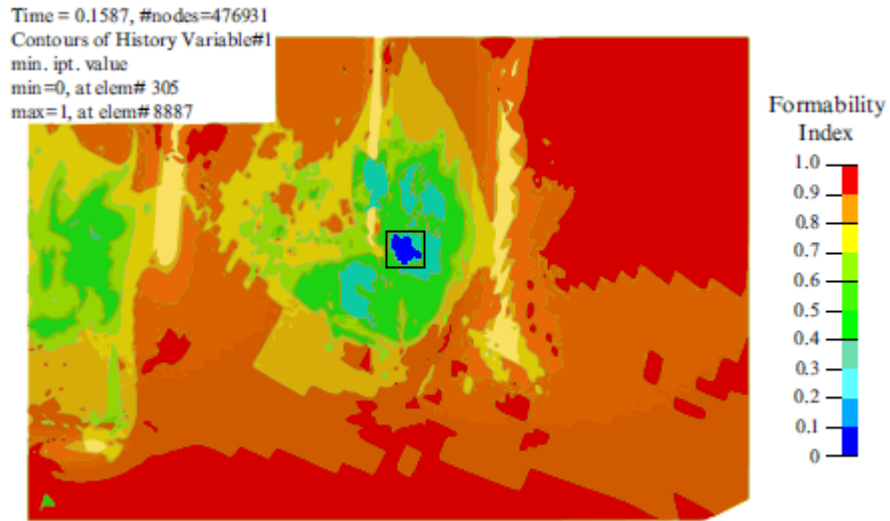


Figure 15. Identify maximum F.I. values with a box.

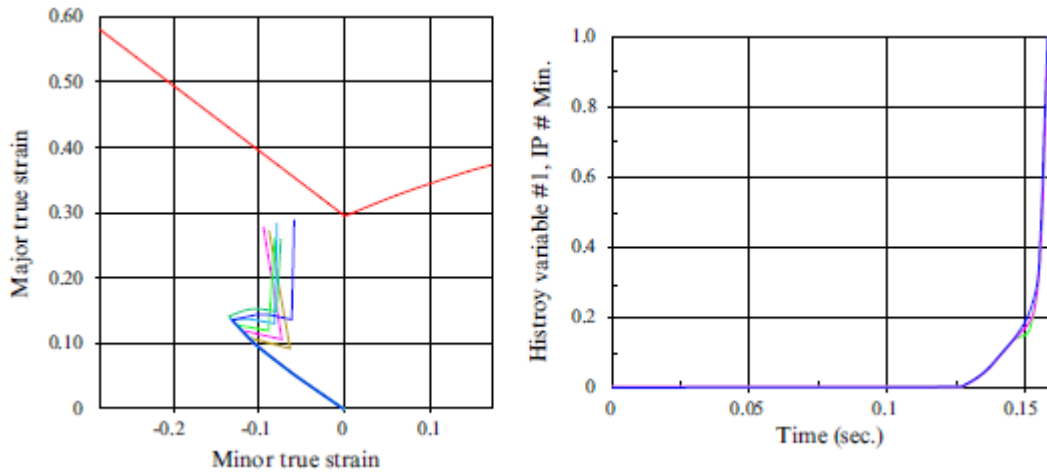


Figure 16. Plot strain paths and F.I. history for the elements within the box.

***MAT_165B**

This material model is implemented to model the cyclic fatigue behavior, and it applies to both shell and solid elements.

This material model is based on a 2013 paper by S. Plessis which modeled a doublenotched specimen with Herbland (2009) material model. The elastoplastic stress tensor is given by:

$$\underline{\sigma} = \underline{\sigma}_M - \underline{L}; \underline{\epsilon}^P$$

where, $\underline{\sigma}_M$ is elastic stress, $\underline{\epsilon}^P$ is the plastic strain tensor. In a one-dimensional problem, the above equation becomes:

$$\sigma = \sigma_M - L' \epsilon^P$$

where, L' is a parameter identified with FEM on a monotonic loading.

In the elasticity domain:

$$f = J_2(\underline{\sigma} - X_T) - R_e - R \leq 0$$

where J_2 is the second stress invariant, σ is the stress tension, R is the isotropic hardening variable, R_e (variable RE) is the yield stress.

Evolution law of the isotropic hardening variable R:

$$\dot{R} = b X(Q - R) \dot{p}$$

where b (variable B) and Q (variable Q) are two material parameters, \dot{p} is the plastic strain rate defined by:

$$\dot{p} = \sqrt{\frac{2}{3} \underline{\dot{\epsilon}}^P : \underline{\dot{\epsilon}}^P}$$

with $\underline{\dot{\epsilon}}^P$ the plastic strain tensor.

Evolution law of the variable of kinematic hardening:

$$\underline{\dot{X}}_T = \sum_i \underline{\dot{X}}_i$$

with,

$$\underline{\dot{X}}_i = \frac{2}{3} C_i \underline{\dot{\epsilon}}^P - \gamma_i X_i \dot{p}$$

where \underline{X}_T is the kinematic hardening tensor, and is the sum of three tensors $X_i (i = 1 \sim 3)$, each dependent on the one set of material coefficients C_i (variables C_1, C_2, C_3) and γ_i (variables GAMMA1, GAMMA2, GAMMA3).

As shown in Figure 17, a cyclic test on a single shell element was conducted. Good comparison was achieved on cyclic behavior between *MAT_165B results and those from the paper.

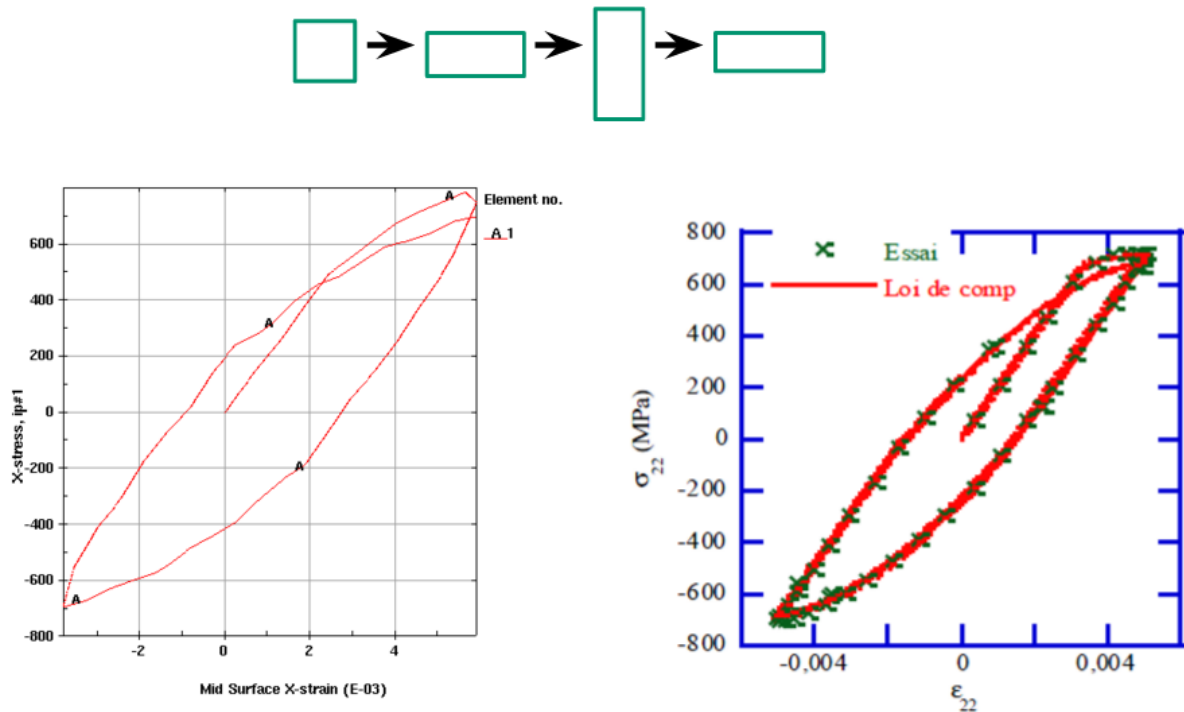


Figure 17. Comparison of cyclic behavior between *MAT_165B and results from the paper.

Summary

Several new features related to metal forming application were developed, tested and applied in production environment over the past two years. LSTC will continue to work with our user community to meet the future challenges facing the metal forming industry.

References

1. *LS-DYNA User's Manual I, II.*